Contents lists available at SciOpen

Food Science and Human Wellness

journal homepage: https://www.sciopen.com/journal/2097-0765

China Food Publishing Co.

An edible green algae polysaccharide from *Caulerpa racemosa* var. *peltate* induced apoptosis of liver cancer cells Hepa1-6 by regulating glutathione metabolism

Xuewei Xia[a,#], Heying Zhou[b,#], Rongxin Zhang[c,d], Xiaoyong Zhang[e], Baojun Xu[f], Io Nam Wong[g,*], Riming Huang[a,*]

[a] *Guangdong Provincial Key Laboratory of Food Quality and Safety, College of Food Science, South China Agricultural University, Guangzhou 510642, China*
[b] *Department of Pharmacy, Guangdong Second Provincial General Hospital, Guangzhou 510317, China*
[c] *Department of Colorectal Surgery, Sun Yat-sen University Cancer Center, Guangzhou 510060, China*
[d] *State Key Laboratory of Oncology in South China, Guangzhou 510060, China*
[e] *Joint Laboratory of Guangdong Province and Hong Kong Region on Marine Bioresource Conservation and Exploitation, College of Marine Sciences, South China Agricultural University, Guangzhou 510642, China*
[f] *Food Science and Technology Program, BNU-HKBU United International College, Zhuhai 519087, China*
[g] *Faculty of Medicine, Macau University of Science and Technology, Macau 999078, China*

ARTICLE INFO

Article history:
Received 3 April 2024
Received in revised form 27 April 2024
Accepted 13 May 2024

Keywords:
Caulerpa racemosa var. *peltate*
Polysaccharide
Anti-liver cancer activity
Metabolism
Mechanism

ABSTRACT

Algal polysaccharides are an essential active substance in food nutrition and even pharmaceutical activity research due to wide sources, low toxicity, and no side effects. In our previous research, we identified the chemical structure and studied the immunomodulatory mechanism of the polysaccharide from edible green algae *Caulerpa racemosa* var. *peltata* (CRVP). In this study, we further investigated the cytotoxicity and potential mechanism of CRVP against Hepa1-6 cells. Metabolomics analysis showed that CRVP might affect glutathione metabolism-related pathways. CRVP significantly up-regulated oxidized glutathione (GSSG) and down-regulated reduced glutathione (GSH) in Hepa1-6 cells, increasing the ratio of GSSG to GSH and intracellular reactive oxygen species. The potential anti-liver cancer mechanism is that CRVP may affect redox homeostasis and lead to apoptosis by inhibiting glutathione reductase or System Xc^-. Based on the known immunomodulatory mechanism of CRVP, this study can provide a material basis for adjuvant therapeutic nutritional agents with immune-enhancing anti-cancer activity.

© 2025 Beijing Academy of Food Sciences. Publishing services by Tsinghua University Press.
This is an open access article under the CC BY-NC-ND license
(http://creativecommons.org/licenses/by-nc-nd/4.0/).

1. Introduction

Cancer, being the second most prevalent cause of mortality on a global scale, presents a substantial menace to both the physical and mental health of individuals[1]. Notable progress achieved in the field of cancer therapy with the development of surgical interventions, radiotherapy, chemotherapy, and targeted therapy[2]. Nevertheless, certain constraints persistently impede the efficacy of these cancer treatments. Based on the 2020 global cancer data published by the International Agency for Research on Cancer (IARC), liver cancer is among the ten most prevalent types of cancer worldwide[3]. The latest available data show that it holds the second-highest mortality rate of liver cancer at 12.3% in China among all cancer types[4]. A large population base and above-average mortality rates make China the

# These authors contributed equally to this work.
* Corresponding authors.
E-mail address: inwong@must.edu.mo (I.N. Wong); huangriming@scau.edu.cn (R. Huang)
Peer review under responsibility of Beijing Academy of Food Sciences.

SciOpen Publishing services by Tsinghua University Press

http://doi.org/10.26599/FSHW.2024.9250300
2213-4530/©2025 Beijing Academy of Food Sciences. Publishing services by Tsinghua University Press. This is an open access article under the CC BY-NC-ND license (http://creativecommons.org/licenses/by-nc-nd/4.0/).

country with the highest number of diagnosed cases globally. Surgical resection, ablation, and liver transplantation are widely regarded as efficacious therapeutic approaches for early-stage liver cancer[5]. Unfortunately, most liver cancers are not detected until advanced stages, and sorafenib is the only approved first-line drug at this time[6]. However, drug resistance and adverse effects remain a key issue hindering its treatment. Therefore, anti-cancer research needs to focus on novel compounds for adjuvant therapy.

Cancer is closely associated with immunity. In the early stage, the organism can target and kill tumor cells through the immune response, thus inhibiting the occurrence and development of tumors. However, most of the tumors can evade immune monitoring[7]. In response to this characteristic, immunotherapy was born. It can kill tumors by activating the patient's immune system, which is a new direction for tumor treatment[8].

Diet regulation has been shown to either limit the unique nutritional requirements of tumors or enhance the effects of anti-cancer drugs. It may provide a novel approach to tumor prevention or adjuvant therapy[9]. There is growing evidence that many dietary natural products are potential sources for the prevention and treatment of liver cancer, including several natural polysaccharides from mushrooms, vegetables, and corn[10]. Polysaccharide from *Lentinula edodes* mycelia (LEP) induced apoptosis of human hepatocellular carcinoma (HCC) cell line HepG2 through caspase-8/-3 death receptor pathways[10-11]. Deproteinized *Asparagus* polysaccharides (ASP) were selectively toxic to HCC cells HepG2 and Hep3B[12]. It can induce apoptosis and enhance the effect of the anti-cancer drug mitomycin *in vitro* and *in vivo*. Yang et al.[13] showed that corn silk polysaccharides (CSP) significantly inhibited tumor growth and extended the survival time of mice bearing HCC H22 cells. CSP might exert an anti-tumor effect to a certain extent through the activation of the immune.

Algal polysaccharides, which are mostly rich in sulfate groups, have a variety of biological activities, including immunomodulatory, anti-cancer, antioxidant, anticoagulant, and antibacterial activity as well as non-toxicity and no side effects[14]. As expected, our group purified a series of polysaccharides rich in sulfate from a large edible green algae *Caulerpa racemosa* var. *peltata* that grows in the tropics and subtropics[15-18]. The purified polysaccharide CRVP-1 was the most abundant fraction via eluting with 0.1 mol/L NaCl solution from the DEAE ion-exchange column, with sulfate content of (25.8 ± 0.7)% and molecular weight of 29.68 kDa[16]. Another fraction named CCP was obtained after elution using 0.6 mol/L NaCl solution, with sulfate content of (42.5 ± 0.4)% and molecular weight of 321.6 kDa[17]. Both of the two fractions were able to significantly increase NO production and inflammatory cytokines secretion in macrophage RAW264.7[17-18].

The immunomodulatory effect of polysaccharide from *C. racemosa* var. *peltata* (CRVP) has been demonstrated. However, the role in tumors requires to be clarified based on the search for novel compounds for adjuvant anti-cancer therapy. Our previous study found that crude CRVP had a cytotoxicity effect on mouse liver cancer cells Hepa1-6 and human HCC cells HepG2, but the mechanism of anti-liver cancer activity remained unclear. Therefore, this study investigated the potential mechanism of CRVP against liver cancer cells by high-throughput techniques including untargeted metabolomics and targeted amino acid metabolomics.

2. Materials and methods

2.1 Preparation of CRVP

The crude CRVP were prepared via our previously reported method[16]. The algae *C. racemosa* var. *peltata* was collected from the sea near Zhanjiang City, Guangdong Province, China. In brief, the air-dried algae powders and water were extracted twice at 85 ℃ in a ratio of 1:30. Filtered the extraction and concentrated it by rotary evaporation at 65 ℃. Then centrifuged at 22 000 × *g* for 10 min, retain supernatant. The deproteinization of supernatant was performed by the Sevag method. The deproteinized supernatant was mixed with three times volumes of anhydrous ethanol overnight. Collected sediment after centrifugation and dissolved it in an appropriate volume of water. Dialyzed against water for 3 days (cut-off molecular weight 8 000 Da). Finally, the dialysate was lyophilized to acquire CRVP. For cellular experiments, the CRVP sample was dissolved in DMEM (Thermo Fisher Scientific, Waltham, MA, USA) supplemented with 10% (*V*/*V*) fetal bovine serum (FBS) and 1% (*V*/*V*) penicillin-streptomycin at the required concentrations and through a 0.22 μm microporous filter membrane. The CRVP solution was prepared on the day of the experiment.

2.2 Cell culture

The HCC cell line HepG2 and mouse liver cancer cell line Hepa1-6 were obtained from Procell Life Science & Technology Co., Ltd. (Wuhan, China). The cells were cultured in an incubator with 5% CO_2 at 37 ℃. The media were MEM for HepG2 cells and DMEM for Hepa1-6 cells, both supplemented with 10% (*V*/*V*) fetal bovine serum (FBS) and 1% (*V*/*V*) penicillin-streptomycin. The abovementioned reagents were purchased from Thermo Fisher Scientific (Waltham, MA, USA).

2.3 Cell viability assay

The cell viability assay of HepG2 and Hepa1-6 cells was detected using a Cell Counting Kit-8 (CCK-8, Yeasen Biotechnology (Shanghai) Co., Ltd., Shanghai, China). The experiments were performed in three replicates. Cells were cultured in 96-well plates at the density of 5×10^3 cells/well. The fresh medium with CRVP at the final concentration of 0 to 10 mg/mL was used to replace the previous medium after 24 h cultured. With an additional 72 h of CRVP treatment, 10 μL/well CCK-8 reagent was added and incubated for 2 h at 37 ℃. Then, the absorbance value at 450 nm was detected. The cell viability (%) was calculated as $(A_{test} - A_{blank})/(A_{control} - A_{blank}) \times 100$, where the A_{test}, $A_{control}$, and A_{blank} represented the absorbance value at 450 nm of the treatment group, control group, and cell-free reagent control, respectively. The half inhibitory concentrations (IC_{50}) of CRVP against liver cancer cells was analyzed and plotted using GraphPad Prism software (v8.0.2).

2.4 Wound-healing assay

The experiment group was set up as the control group, and the CRVP treatment group (3.5 mg/mL CRVP). Each group used the low-serum medium (with 2% fetal bovine serum). Cells were cultured

in a 6-well plate at a density of 5×10^5 cells/well and placed in an incubator for 24 h until the cell state stabilized. Using the 10 μL pipette tip uniformly scratches a line on a monolayer of dense cells. The photos were taken with a microscope to record the change of scratches at 0, 12, and 24 h. The photos were analyzed by the software ImageJ v1.53t, the edges of the scratched area were marked with yellow curves. The area of the scratched area is marked as A. The scratch area at 0 h (A_0) was used as a reference for each position to calculate the scratch closure rate at 12 or 24 h. The scratch closure rate (%) equaled to $(A_0 - A)/A_0 \times 100$.

2.5 Metabolomics analysis

Metabolomic analyses were performed according to previously reported methods[19]. The experiment contained the control group (0 mg/mL CRVP) and CRVP treatment group (7 mg/mL CRVP) with three replicates. The cells were collected after 72 h treated and immediately quenched in liquid nitrogen.

The cell samples were added 1 000 μL water solution of 40% acetonitrile and 40% methanol (*V/V*). Cells were broken with the pulses of vortexing using 100 mg glass beads for 30 s, then were milled at 55 Hz for 2 min three times, with a 5-min hold on liquid nitrogen between each milling. After cell crushing, the cells were centrifuged for 10 min at 12 000 r/min and 4 ℃ and concentrated and dried all supernatant. Redissolve the sample in 300 μL of acetonitrile containing 0.04% 2-amino-3-(2-chloro-phenyl)-propionic acid and 0.09% formic acid (*V/V*). Then, the sample was filtered through a 0.22 μm membrane.

Liquid chromatography-tandem mass spectrometry (LC-MS/MS) analysis for non-targeted metabolomics was performed on a Waters ACQUITY UPLC HSS T3 column (1.8 μm, 2.1 mm × 100 mm) and a Waters ACQUITY UPLC BEH Amide column (1.7 μm, 2.1 mm × 100 mm). LC-MS/MS analysis for targeted amino acid metabolomics was performed on a Waters ACQUITY BEH Amide column (1.7 μm, 2.1 mm × 100 mm).

The orthogonal partial least squares-discriminant analysis (OPLS-DA) models were built via ropls package on R language (v1.3.959), and the variable importance in the projection (VIP) values were derived from it. The *P*-value was obtained by the Wilcoxon-Mann-Whitney test. The fold change (FC) was calculated as the mean relative or absolute metabolite content in the CRVP treatment group divided by that in the control group. The $\log_2$ FC denoted the logarithm of FC with a base of two. Its positive or negative values represented the up- or down-regulation of the CRVP treatment group relative to the control group, respectively. The metabolites with VIP value > 1 and $|\log_2 FC| > 1$ in non-targeted metabolomics were considered as significant differential accumulated metabolites (DAMs). The metabolites with $P < 0.05$ and $|\log_2 FC| > 1$ in targeted amino acid metabolomics were considered as significant DAMs. Subsequently, Kyoto Encyclopedia of Genes and Genomes (KEGG) pathway analysis was carried out on all significant DAMs by MetaboAnalyst v5.0.

2.6 Determination of reduced glutathione (GSH) and oxidized glutathione (GSSG) content

The content of GSH and GSSG were determined according to the instructions of the kit (Solarbio, Beijing, China). Cultured 1×10^7 cells in 6-well plates for the experiment of the control group and CRVP treatment group (3.5 mg/mL or 7 mg/mL CRVP). The measurements were carried out in triplicate. Before using the kit, a cell count was performed to correct the results.

2.7 Measurement of reactive oxygen species (ROS) and lipid peroxidation levels

The ROS and lipid peroxidation levels were detected by flow cytometry using the fluorescent probe of 2′,7′-dichlorodihydrofluorescein diacetate (DCFH-DA) (Solarbio, Beijing, China) and BODIPY 581/591 C11, respectively. The experiments were carried out with three replicates. After treatment, the medium in 6-well plates was replaced by a non-serum medium with fluorescent probe solution at a final concentration of 10 μmol/L DCFH-DA or 2 μmol/L BODIPY 581/591 C11. With 20 min of incubation, cells were harvested and resuspended in the non-serum medium at a density of 6×10^5 cells/mL. Then, the flow cytometry was performed to obtain the fluorescence intensity. The results were analyzed by FlowJo v10.3 software.

2.8 Western blot

After treatment, lysed cells in the 1× phenylmethanesulfonyl fluoride (PMSF) with radio immunoprecipitation assay (RIPA) lysis buffer (Beyotime, Shanghai, China). The protein (20 μg) was electrophoresed in each lane on a 10% Bis-Tris sodium dodecyl sulfate-polyacrylamide gel electrophoresis (SDS-PAGE) gel. Transferred protein to nitrocellulose membranes. The membranes were incubated in 1× Tris buffered saline Tween (TBST) containing 5% bovine serum albumin at room temperature for 1 h, then incubated in the primary antibody (rabbit antibodies) solutions at 4 ℃ overnight, including GAPDH (Bioworld Technology, Nanjing, China), acyl-CoA synthetase long-chain family member 4 (ACSL4, #DF12141, Affinity Biosciences, OH, USA), and 15-lipoxygenase (ALOX15, #DF13494, Affinity Biosciences, OH, USA). Further incubation was performed with goat anti-rabbit antibodies at room temperature for 1 h. Before developing with enhanced chemiluminescence (Amersham Life Science, TX, USA), the blots were washed in 1× TBST three times at room temperature for 10 min. Using the BeyoECL Star kit (Beyotime, Shanghai, China) enhanced chemiluminescence.

2.9 Annexin V-fluorescein isothiocyanate (FITC)/propidium iodide (PI) double staining

The experiment group contained the control group, CRVP treatment group (3.5 or 7 mg/mL CRVP), cell death inhibitor group, and CRVP combined with cell death inhibitor group. The apoptosis inhibitor Z-VAD-FMK (50 μmol/L), necrosis inhibitor necrostatin-1 (Nec-1, 50 μmol/L), or ferroptosis inhibitor ferrostatin-1 (Fer-1, 5 μmol/L) cell death inhibitor was applied for cell death inhibitor. After treatment, the cells were harvested by trypsin without ethylenediaminetetraacetic acid (EDTA) and resuspended in phosphate buffered saline (PBS) at the density of 1×10^5 cells/mL. A 100 μL of cell suspension and 5 μL of Annexin V-FITC solution were added to the flow tube and incubated for 5 min at room temperature avoiding light. Then 5 μL of PI solution and 400 μL of PBS were added and immediately flow cytometry was detected. The results were analyzed in FlowJo v10.3 software.

2.10 Statistical analysis

The mathematical-statistical analysis and graphing were performed by GraphPad Prism v8.0.2 software. One-way analysis of variance (ANOVA) was used for comparison between the different groups. The *P*-values less than 0.05 were considered statistically significant.

3. Results

3.1 Cell viability of CRVP on liver cancer cells

As demonstrated in Figs. 1a–b, the cell viability of both cell lines showed a decreasing trend as the concentration of CRVP increased. At low concentrations of 1 to 2 mg/mL, the cell viability of HepG2 was maintained at around 90%–100%, whereas the cell viability of Hepa1-6 decreased relatively rapidly. The IC_{50} of CRVP on HepG2 and Hepa1-6 were 5.678 and 3.454 mg/mL, respectively. The IC_{50} of Hepa1-6 was lower in the two cell lines, indicating that the inhibitory effect of CRVP was better on Hepa1-6.

3.2 Effect of CRVP on cell migration ability for Hepa1-6 cells

Primary liver cancer is prone to metastasis, therefore migration is also an essential characteristic of it[20]. In this part, a scratch assay was conducted for the cell migration ability, and the change in the scratched area was expressed as the rate of scratch closure. Hepa1-6 was selected for further experiment, which is more sensitive to CRVP. The concentration of the CRVP treatment group was at IC_{50} (3.5 mg/mL).

As shown in Fig. 1c, the yellow curve is the edge of the scratched area through the software ImageJ v1.53t. With the increase of time, more cells migrated to the scratch area and the cell edges were more curved in the control group than in the CRVP treatment group. There was a significant difference in the scratch closure rate between the control and CRVP treatment groups at 24 h, which was 33% and 17%, respectively (Fig. 1d). The results suggested that CRVP can inhibit cell migration of Hepa1-6.

3.3 Untargeted metabolomics results

Metabolites are critical for cellular function. Untargeted metabolomics allows high-throughput qualitative screening of as many metabolites as possible with a broader coverage. Based on the inhibitory effect of CRVP on Hepa1-6, in this paper, we used untargeted metabolomics for the preliminary screening of differential metabolites to explore the metabolic changes. Based on the inhibitory effect of CRVP on Hepa1-6, untargeted metabolomics was conducted for the initial screening of differential metabolites to investigate the intracellular metabolic changes. The OPLS-DA resuls showed that the control group (0 mg/mL CRVP) and CRVP treatment group (7 mg/mL CRVP) were separated, proving that the results were reliable (Fig. 2a). VIP was obtained from the OPLS-DA models. The absolute value of $\log_2$ FC indicated the degree of change, with positive and negative values representing up- or down-regulated DAMs, respectively. In total, 604 metabolites were identified by LC-MS/MS, of which 123 metabolites were defined as the DAMs by VIP > 1 and $|\log_2 FC| > 1$ (Table S1). Compared with the control group, 8 DAMs

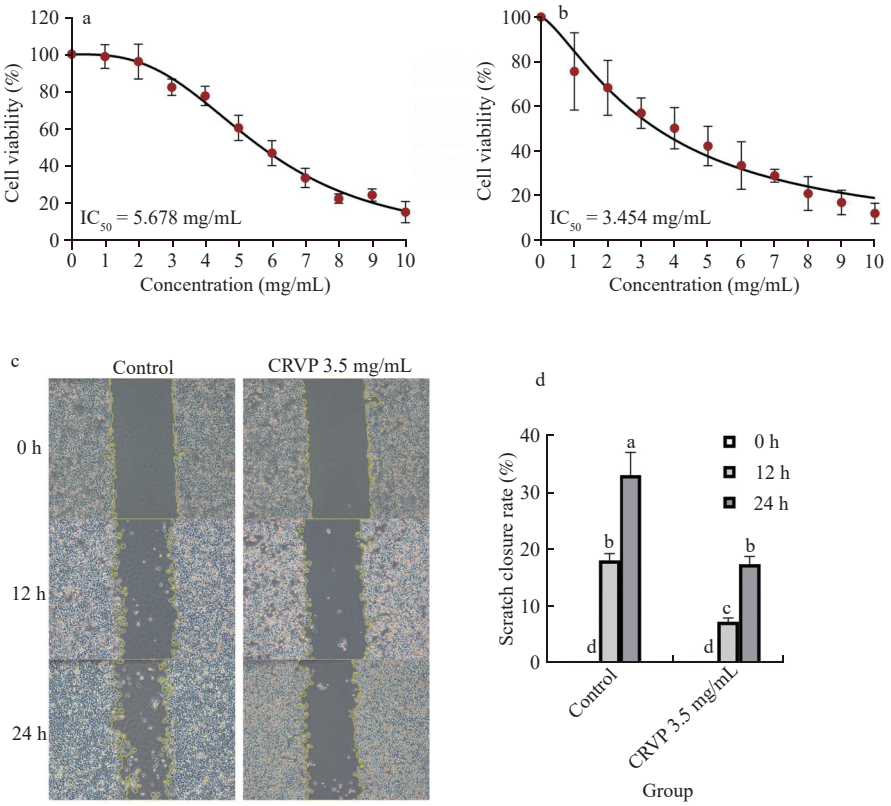


Fig. 1 Cell viability and migration ability of CRVP against liver cancer cells. Cell viability of (a) HepG2 and (b) Hepa1-6 treated with CRVP. (c) The representative picture under the microscope. (d) Scratch closure rate measured by software ImageJ v1.53t. Different letters represent significant differences ($P < 0.05$).

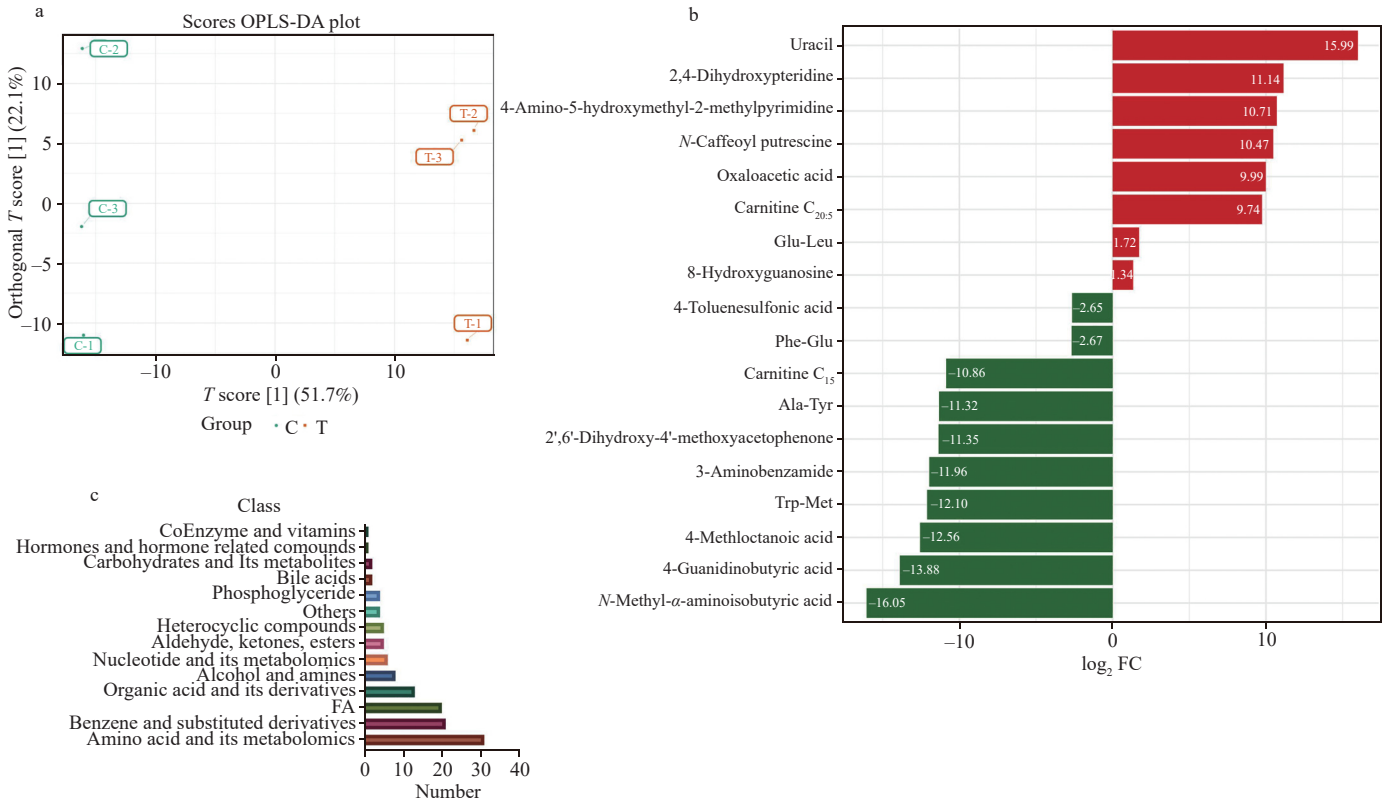


Fig. 2 Untargeted metabolomics analysis of CRVP against Hepa1-6. (a) OPLS-DA score plot. (b) Bar plot of the top 8 up- or top 10 down-regulated DAMs sorted by $\log_2$ FC. The red and green bars represented up- and down-regulated, respectively. (c) Primary classification of DAMs in the KEGG database. C and T represent the control group and the treatment group, respectively.

were up-regulated ($\log_2$ FC > 1) and 115 DAMs were down-regulated ($\log_2$ FC < –1). The top eight up- and top ten down-regulated differential metabolites ranked by $\log_2$ FC were illustrated in Fig. 2b. The primary classification of DAMs was subsequently annotated in KEGG database. All DAMs relate to 14 primary classifications (Fig. 2c). With the highest number of DAMs, the primary classification amino acid and its metabolomics contained 31 differential metabolites, followed by benzene and substituted derivatives and fatty acyls (FA). The above results of untargeted metabolomics analysis demonstrated that the amino acids metabolism was mainly changed in the CRVP treatment group.

3.4 *Targeted amino acid metabolomics analysis*

Since CRVP mainly caused changes in amino acid metabolism in Hepa1-6, we used targeted amino acid metabolomics for absolute quantification. The targeted amino acid metabolomics detected 94 amino acids and their metabolites in total. As shown in Fig. 3a, the control and treatment groups were separated from each other in the OPLS-DA model, and the samples within the group were gathered close. As a result of comparison with the standards, 66 metabolites were finally identified. Using $P < 0.05$ and $|\log_2 \text{FC}| > 1$, the 42 DAMs screened of targeted amino acid metabolomics were listed in Table S2, including 3 up-regulated and 39 down-regulated DAMs. Among them, 2 metabolites detectable only in the CRVP treatment group were defined as up-regulated DAMs, while 5 metabolites detectable only in the control group were defined as down-regulated DAMs. The quantification of all differential metabolites was visualized by clustering heatmaps (Fig. 3b). It is similar to the results of untargeted metabolomics that there are much more down-regulated than up-regulated DAMs. A total of 99 KEGG pathways were annotated for all DAMs, and only the top 20 enriched pathways were shown in Fig. 3c sorted by *P*-value. The most significantly enriched pathways included aminoacyl-tRNA biosynthesis, biosynthesis of amino acids, protein digestion and absorption, mineral absorption, central carbon metabolism in cancer, and *D*-amino acid metabolism ($P < 0.1$).

Among the DAMs, we found ten metabolites associated with the glutathione antioxidant system, whose $\log_2$ FC were shown in Fig. 3d, involving glutathione synthesis and trans-sulfuration pathway. The glutathione synthesis provides reductants to eliminate excess oxidants produced during physiological processes. The trans-sulfuration pathway is one of the sources of cysteine, an important precursor for glutathione synthesis. Changes in these metabolites may affect intracellular redox balance.

3.5 *CRVP broke the homeostasis of GSH and GSSG*

GSSG was one of the only three up-regulated differential metabolites with the largest $\log_2$ FC value. It was the product of GSH after exerting the antioxidant effect. The ratio of GSSG to GSH (GSSG/GSH) had been used as an important indicator of cellular redox homeostasis. Since quantitative results of GSSG show significant up-regulated in targeted amino acid metabolomics, but there is no result for GSH, we performed GSH and GSSG content measurements to explore the changes in GSH and GSSG homeostasis in Hepa1-6 after CRVP treatment.

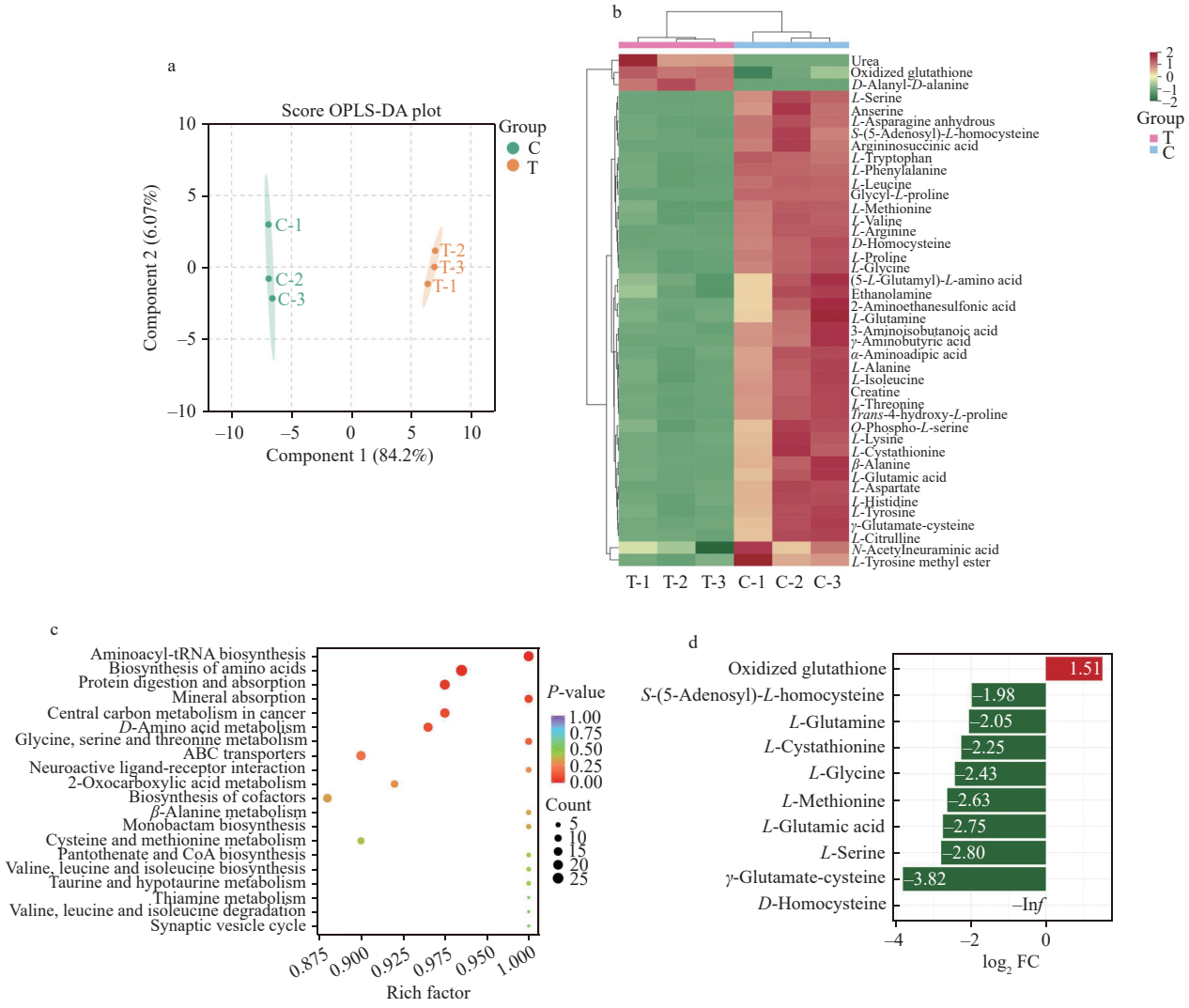


Fig. 3 Targeted amino acid metabolomics analysis of CRVP against Hepa1-6. (a) OPLS-DA score plot. (b) Clustering heat map of DAMs. Shades of color indicated the relative value of $\log_2$ FC after normalization. (c) The top 20 enriched KEGG pathways sorted by *P*-value. (d) The $\log_2$ FC value of ten metabolites associated with the glutathione antioxidant system. –In*f* represents that the metabolite was down-regulated detectable only in the control group and could not be calculated for the value of $\log_2$ FC. C and T represent the control group and the treatment group respectively.

As shown in Figs. 4a–b, the GSH and GSSG contents showed a decreasing and increasing trend with increasing CRVP concentration, respectively. Although the decrease in GSH content was very slight, GSSG rose approximately 4-fold with a high concentration (7 mg/mL) of CRVP compared to the control group. The rise in GSSG content was consistent with the previous results of targeted amino acid metabolomics. As a result, the ratio of GSSG to GSH increased significantly (Fig. 4c). Noda et al.[21] found that a rise in the ratio of GSSG to GSH would lead to proliferation inhibition, which is not dependent on ROS production. Consequently, a significant increase in the ratio of GSSG to GSH after CRVP treatment may result in the proliferation inhibition of Hepa1-6 cells.

3.6 CRVP Induced ROS accumulation rather than lipid peroxidation

The intracellular redox state may be altered by the increase in the ratio of GSSG to GSH, such as ROS accumulation or lipid peroxidation. These alterations may eventually lead to cell death. Excess ROS can induce apoptosis or necrosis, which will depend on the amount of ROS accumulated, and lipid peroxidation may cause ferroptosis[22]. Therefore, we further explored whether CRVP induced alterations of the redox state in Hepa1-6 cells.

It is demonstrated in Fig. 4d that there was no significant change in ROS levels between the 3.5 mg/mL CRVP treatment group and the control group. While the 7 mg/mL CRVP treatment group significantly enhanced the ROS levels.

As for the lipid peroxidation, we found that CRVR can up-regulate the level of two key enzymes, ACSL4 and ALOX15 (Fig. 4e). However, there were no significant differences when we determined the lipid peroxidation level using the fluorescent probe BODIPY 581/591 C11 by flow cytometry (Fig. 4f). The results illustrated that the type of cell death in Hepa1-6 cells was not lipid peroxidation-induced ferroptosis.

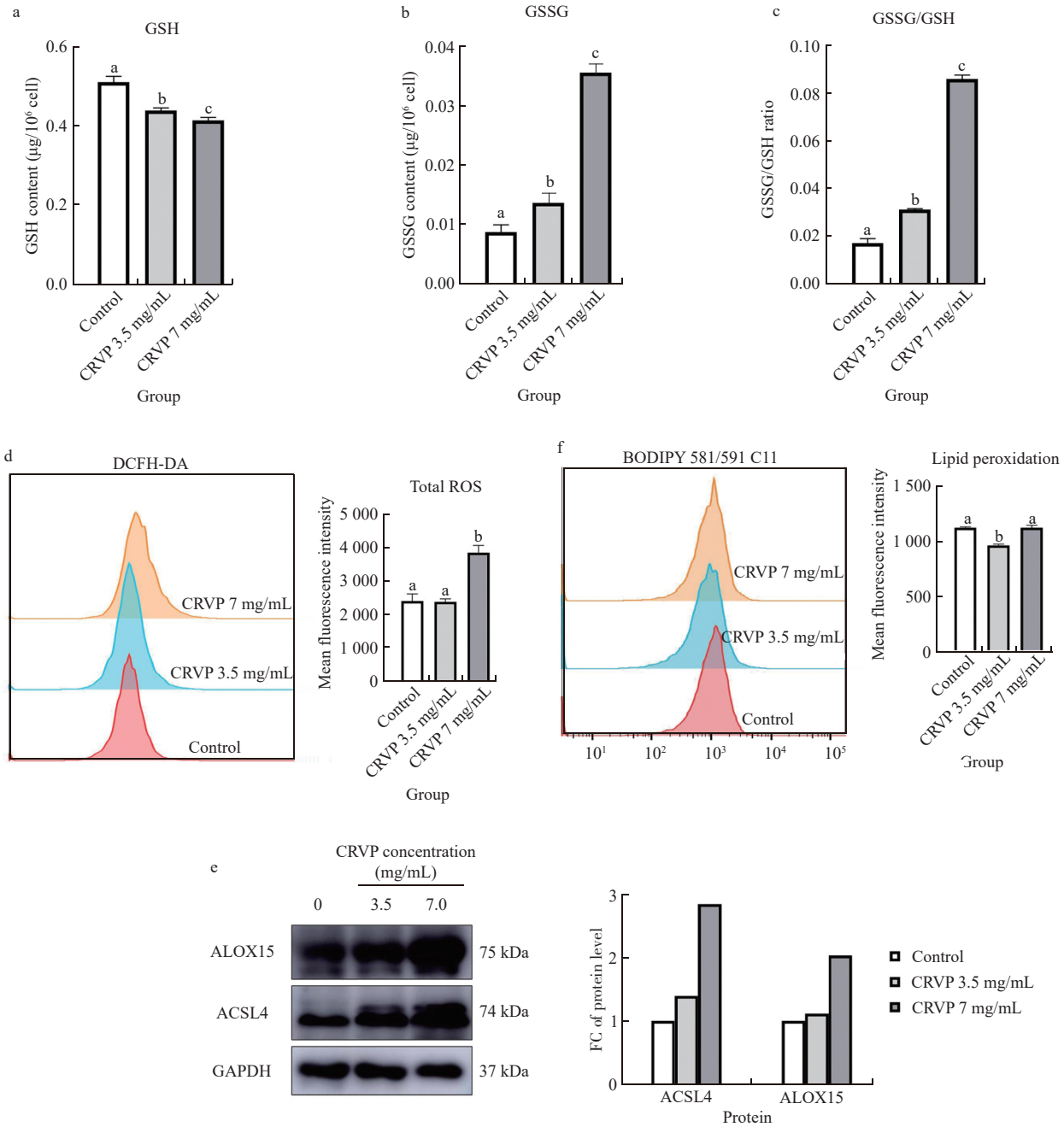


Fig. 4 The effect of CRVP on GSH and GSSG content and intracellular redox state in Hepa1-6 cells. (a) GSH content. (b) GSSG content. (c) The ratio of GSSG to GSH. (d) ROS levels by flow cytometry with the fluorescent probe DCFH-DA. (e) FC of protein levels for ACSL4 and ALOX15. (f) Lipid peroxidation level by flow cytometry with the fluorescent probe BODIPY 581/591 C11. Different letters represent significant differences ($P < 0.05$).

3.7 CRVP induces apoptosis via ROS

CRVP caused an imbalance in the ratio of GSSG to GSH leading to the upregulation of ROS in Hepa1-6 cells, but the specific type of cell death was still unknown. In this section, three possible types of cell death related to an imbalance in the ratio of GSSG to GSH were investigated through flow cytometry Annexin V-FITC/PI staining. Hepa1-6 cells were treated by 7 mg/mL CRVP in combination with apoptosis inhibitor Z-VAD-FMK (50 μmol/L), Nec-1 (50 μmol/L), or Fer-1 (5 μmol/L), respectively. In the results of Annexin V-FITC/PI staining. All the cells will be categorized into 3 types: Q2 (Annexin V-FITC$^+$/PI$^+$), late apoptotic or necrotic cells; Q3 (Annexin V-FITC$^+$/PI$^-$), early apoptotic cells; Q4 (Annexin V-FITC$^-$/PI$^-$), normal cells. Fig. 5 demonstrats that the ratio of normal cells decreased from 90.5% in the control group to 70.9% in the medium concentration group (3.5 mg/mL CRVP) and 52.8% in the high concentration group (7.0 mg/mL CRVP), respectively. Under CRVP combined with cell death inhibitor co-treatment, Z-VAD-FMK was able to rescue the CRVP-induced decrease of cells in the Q4 area, whereas Nec-1 and Fer-1 resulted in fewer cells distributed in the Q4 area (Fig. 5).

It is thus clear that CRVP was mainly through ROS accumulation leading to oxidative stress, which ultimately induces apoptosis rather

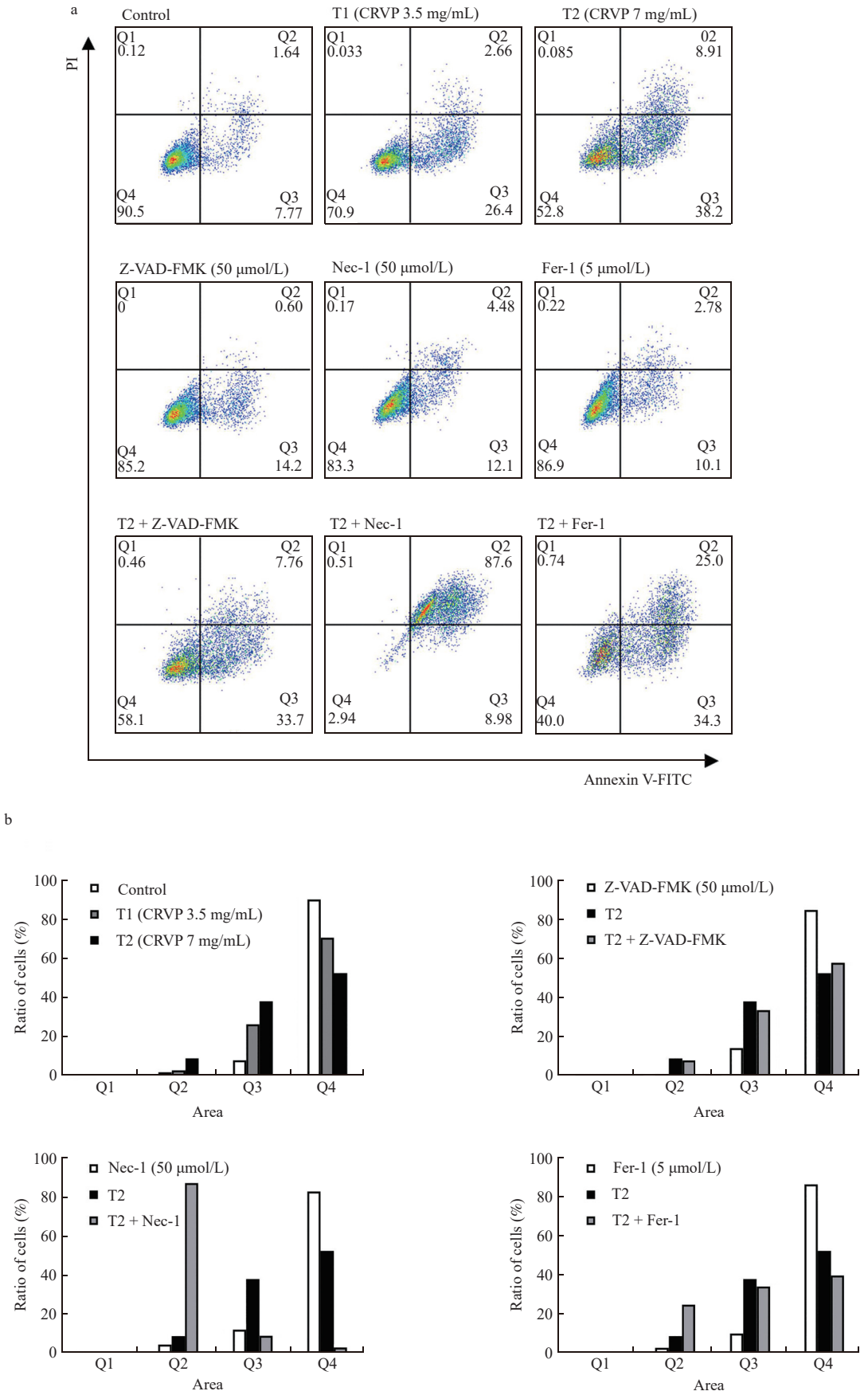


Fig. 5 The type of cell death induced by CRVP in Hepa1-6 cells. (a) Scatter plot by flow cytometry. (b) Bar plot of cell ratio in each area.

than necrosis. In addition, corresponding to the previous results, the CRVP-induced cell death was also not ferroptosis triggered by lipid peroxidation. For the slightly rescued effect of Z-VAD-FMK from apoptosis, we speculated that it was related to the high concentration of CRVP.

4. Discussion

The glutathione antioxidant system was one of the most important defenses against oxidative stress, and included two essential members of GSH and GSSG[23]. Increased GSH levels were commonly observed in different cancers, whereas oxidative stress due to GSH depletion enhanced the sensitivity to various programmed cell death and chemotherapy[24]. Glutathione antioxidant system may be a potential target for therapies against cancer[25].

In this study, the effect of CRVP against liver cancer cells Hepa1-6 may be related to the upregulation in the ratio of GSSG to GSH in the glutathione antioxidant system, while GSSG was significantly up-regulated and GSH was down-regulated. GSH was the main form of intracellular glutathione besides the endoplasmic reticulum, and only a few GSSG existed[26]. The up-regulation of GSSG present illustrated the function of conversion from GSH to GSSG was normal in CRVP-treated Hepa1-6 cells. Hence, the discussion of the possible mechanism for CRVP against liver cancer cells Hepa1-6 will focus on both the reduction reaction of GSSG and the synthesis of GSH in the glutathione antioxidant system. The key metabolites and enzymes involved in this system are illustrated in Fig. 6.

On one hand, inhibition of the GSSG reduction reaction would cause GSSG accumulation. The reduction reaction of GSSG, catalyzed by glutathione reductase (GR), was as important as the presence of the oxidation reaction of GSH. This reaction allowed to regeneration of GSH from GSSG, which helps to maintain a reducing intracellular environment and prevents the overaccumulation of GSSG[27]. It was an essential source of GSH for the place where no *de novo* synthesis occurred. GR inhibition had been shown to lead to the accumulation of GSSG, rapid GSH depletion, and the generation of intracellular ROS, which is one of the potential targets for current cancer therapy[28].

Li et al.[29] used an irreversible GR inhibitor to induce thiol oxidative stress, inhibit cell growth of mouse melanoma cells B16F10 *in vitro*, and suppress subcutaneous tumor cell growth and lung metastasis *in vivo*. Hwang et al.[30] demonstrated that plumbagin can directly inhibit GR and thioredoxin reductase, generate intracellular ROS, and induce apoptosis, thus exerting its anticancer effects. Similar to the above studies, the results of the targeted amino acid metabolomics and GSSG content showed up-regulation of GSSG in CRVP-treated Hepa1-6 cells. It suggested that inhibition of GR may occur so that GSSG accumulated leading to thiol oxidative stress in the cells.

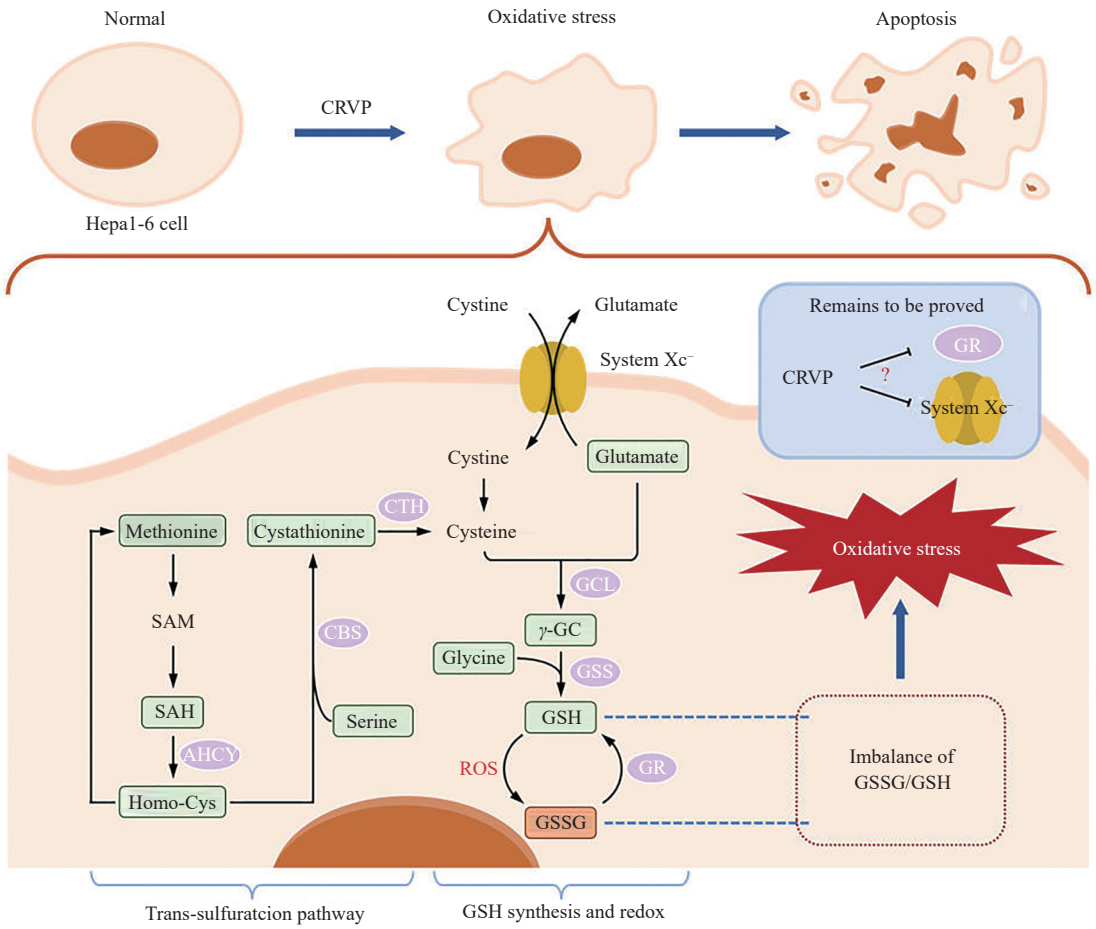


Fig. 6 Potential mechanism of CRVP-induced apoptosis in Hepa1-6 cells via glutathione antioxidant system. The green and red-filled boxes represented down- and up-regulated metabolites, respectively. The purple round boxes represent key enzymes in the pathway. AHCY: adenosylhomocysteinase; CBS: cystathionine beta-synthase; CTH: cystathionase.

On the other hand, the lack of a key precursor would lead to a decrease in *de novo* GSH synthesis. GSH is a tripeptide composed of glutamic acid, cysteine, and glycine[31]. The synthesis of GSH began with the generation of γ-glutamylcysteine (γ-GC) from glutamate and cysteine catalyzed by glutamate cysteine ligase (GCL), which was subsequently linked to glycine for generating GSH catalyzed by glutathione synthetase (GSS).

Among the 3 materials, cysteine was the limiting factor for GSH synthesis[32]. Intracellular cysteine was mainly derived from the cystine transported into the cell via the cystine/glutamate antiporter (System Xc^-), which was then reduced to cysteine. In addition, the trans-sulfuration pathway of methionine can also provide some of the cysteine for GSH synthesis. It generally compensated for cysteine depletion when system Xc^- was inhibited. In the trans-sulfuration pathway, methionine was sequentially converted to *S*-adenosylmethionine (SAM), *S*-adenosylhomocysteine (SAH), homo-cysteine (Homo-Cys), cystathionine, and ultimately cysteine under multiple enzymes[33-34].

As shown in Table S2, the results of targeted amino acid metabolomics showed a downregulation of the precursor for GSH synthesis in CRVP-treated Hepa1-6 cells, including glutamate, cysteine, glycine, and γ-GC. The synthetic material of GSH was lacking. Moreover, metabolites of the trans-sulfuration pathway containing methionine, SAH, Homo-Cys, and cystathionine were down-regulated. The conversion of methionine to cysteine may occur. And GSH was down-regulated due to the lack of synthetic precursor eventually. It was indicated that system Xc^- might be one of the targets in CRVP against Hepa1-6 cells.

5. Conclusion

In summary, CRVP had an anti-liver cancer effect on Hepa1-6 cells and upregulated the ratio of GSSG to GSH and ROS level to induce apoptosis. The potential mechanism of CRVP on Hepa1-6 cells may regulate the glutathione antioxidant system via inhibiting GR or system Xc^- to exert the anti-liver cancer activity. However, there were still some limitations in this study. On one hand, the specific pathways of its inhibition remained to be further clarified. On the other hand, although the anti-liver cancer and immunomodulatory properties of CRVP have been confirmed, the interaction between tumor cells and immune cells remains to be further demonstrated.

Declaration of interest

Baojun Xu is an associate editor for *Food Science and Human Wellness* and was not involved in the editorial review on the decision to publish this article. The authors have declared that no competing interest exists.

Acknowledgements

This research was funded by the National Natural Science Foundation of China (32161160304 and 32272241); the Macau Science and Technology Development Fund (0069/2021/AFJ); and the Key-Area Research and Development Program of Guangdong Province (2022B0202020004).

Appendix A. Supplementary information

Supplementary data associated with this article can be found, in the online version, at http://doi.org/10.26599/FSHW.2024.9250300.

References

[1] J. Cortes, J.M. Perez-Garcia, A. Llombart-Cussac, et al., Enhancing global access to cancer medicines, Ca-Cancer J. Clin. 70 (2020) 105-124. https://doi.org/10.3322/caac.21597.

[2] K.D. Miller, R.L. Siegel, C.C. Lin, et al., Cancer treatment and survivorship statistics, Ca-Cancer J. Clin. 66 (2016) 271-289. https://doi.org/10.3322/caac.21349.

[3] J. Ferlay, M. Colombet, I. Soerjomataram, et al., Cancer statistics for the year 2020: an overview, Int. J. Cancer 149 (2021) 778-789. https://doi.org/10.1002/ijc.33588.

[4] J. Ferlay, M. Ervik, F. Lam, et al., Global cancer observatory: cancer today. Lyon, France: International Agency for Research on Cancer, 2024. https://gco.iarc.who.int/today.

[5] Z. Lin, Y. Niu, A. Wan, et al., RNA m(6) a methylation regulates sorafenib resistance in liver cancer through foxo3-mediated autophagy, EMBO J. 39 (2020) e103181. https://doi.org/10.15252/embj.2019103181.

[6] D. Anwanwan, S.K. Singh, S. Singh, et al., Challenges in liver cancer and possible treatment approaches, Biochim. Biophys. Acta-Rev. Cancer 1873 (2020) 188314. https://doi.org/10.1016/j.bbcan.2019.188314.

[7] X. Lei, Y. Lei, J.K. Li, et al., Immune cells within the tumor microenvironment: biological functions and roles in cancer immunotherapy, Cancer Lett. 470 (2020) 126-133. https://doi.org/10.1016/j.canlet.2019.11.009.

[8] M. Abbott, Y. Ustoyev, Cancer and the immune system: the history and background of immunotherapy, Semin. Oncol. Nurs. 35 (2019) 150923. https://doi.org/10.1016/j.soncn.2019.08.002.

[9] N. Kanarek, B. Petrova, D.M. Sabatini, Dietary modifications for enhanced cancer therapy, Nature 579 (2020) 507-517. https://doi.org/10.1038/s41586-020-2124-0.

[10] Y. Zhou, Y. Li, T. Zhou, et al., Dietary natural products for prevention and treatment of liver cancer, Nutrients 8 (2016) 156. https://doi.org/10.3390/nu8030156.

[11] H. Yukawa, S. Ishikawa, T. Kawanishi, et al., Direct cytotoxicity of *Lentinula edodes* mycelia extract on human hepatocellular carcinoma cell line, Biol. Pharm. Bull. 35 (2012) 1014-1021. https://doi.org/10.1248/bpb.b110657.

[12] J. Xiang, Y. Xiang, S. Lin, et al., Anticancer effects of deproteinized *Asparagus* polysaccharide on hepatocellular carcinoma *in vitro* and *in vivo*, Tumour Biol. 35 (2014) 3517-3524. https://doi.org/10.1007/s13277-013-1464-x.

[13] J. Yang, X. Li, Y. Xue, et al., Anti-hepatoma activity and mechanism of corn silk polysaccharides in H22 tumor-bearing mice, Int. J. Biol. Macromol. 64 (2014) 276-280. https://doi.org/10.1016/j.ijbiomac.2013.11.033.

[14] Y. Ouyang, Y. Qiu, Y. Liu, et al., Cancer-fighting potentials of algal polysaccharides as nutraceuticals, Food Res. Int. 147 (2021) 110522. https://doi.org/10.1016/j.foodres.2021.110522.

[15] H.L. Hao, M.Q. Fu, R. Yan, et al., Chemical composition and immunostimulatory properties of green alga *Caulerpa racemosa* var. *peltata*, Food Agric. Immunol. 30 (2019) 937-954. https://doi.org/10.1080/09540105.2019.1646216.

[16] H. Hao, Y. Han, L. Yang, et al., Structural characterization and immunostimulatory activity of a novel polysaccharide from green alga *Caulerpa racemosa* var. *peltata*, Int. J. Biol. Macromol. 134 (2019) 891-900. https://doi.org/10.1016/j.ijbiomac.2019.05.084.

[17] Y. Wu, J. Liu, H. Hao, et al., A new polysaccharide from *Caulerpa chemnitzia* induces molecular shifts of immunomodulation on macrophages RAW264.7, Food Chem. X 14 (2022) 100313. https://doi.org/10.1016/j.fochx.2022.100313.

[18] X. Xia, H. Hao, X. Zhang, et al., Immunomodulatory sulfated polysaccharides from *Caulerpa racemosa* var. *peltata* induces metabolic

shifts in NF-κB signaling pathway in RAW264.7 macrophages, Int. J. Biol. Macromol. 182 (2021) 321-332. https://doi.org/10.1016/j.ijbiomac.2021.04.025.

[19] W.J. Jang, B. Choi, S.H. Song, et al., Multi-omics analysis reveals that ornithine decarboxylase contributes to erlotinib resistance in pancreatic cancer cells, Oncotarget 8 (2017) 92727-92742. https://doi.org/10.18632/oncotarget.21572.

[20] C. Liang, W. Li, H. Ge, et al., Role of Beclin1 expression in patients with hepatocellular carcinoma: a meta-analysis, Oncotargets Ther. 11 (2018) 2387-2397. https://doi.org/10.2147/OTT.S151751.

[21] T. Noda, R. Iwakiri, K. Fujimoto, et al., Induction of mild intracellular redox imbalance inhibits proliferation of Caco-2 cells, FASEB J. 15 (2001) 2131-2139. https://doi.org/10.1096/fj.01-0131com.

[22] C. Tonelli, I. Chio, D.A. Tuveson, Transcriptional regulation by Nrf2, Antioxid. Redox Signal. 29 (2018) 1727-1745. https://doi.org/10.1089/ars.2017.7342.

[23] H. Lv, C. Zhen, J. Liu, et al., Unraveling the potential role of glutathione in multiple forms of cell death in cancer therapy, Oxid. Med. Cell. Longev. 2019 (2019) 3150145. https://doi.org/10.1155/2019/3150145.

[24] N. Traverso, R. Ricciarelli, M. Nitti, et al., Role of glutathione in cancer progression and chemoresistance, Oxid. Med. Cell. Longev. 2013 (2013) 972913. https://doi.org/10.1155/2013/972913.

[25] J. Lee, J. Kim, R. Lee, et al., Therapeutic strategies for liver diseases based on redox control systems, Biomed. Pharmacother. 156 (2022) 113764. https://doi.org/10.1016/j.biopha.2022.113764.

[26] V. Ribas, C. Garcia-Ruiz, J.C. Fernandez-Checa, Glutathione and mitochondria, Front. Pharmacol. 5 (2014) 151. https://doi.org/10.3389/fphar.2014.00151.

[27] N. Couto, J. Wood, J. Barber, The role of glutathione reductase and related enzymes on cellular redox homoeostasis network, Free Radic. Biol. Med. 95 (2016) 27-42. https://doi.org/10.1016/j.freeradbiomed.2016.02.028.

[28] C. Cereser, S. Boget, P. Parvaz, et al., Thiram-induced cytotoxicity is accompanied by a rapid and drastic oxidation of reduced glutathione with consecutive lipid peroxidation and cell death, Toxicology 163 (2001) 153-162. https://doi.org/10.1016/s0300-483x(01)00401-2.

[29] X. Li, J. Wu, X. Zhang, et al., Glutathione reductase-mediated thiol oxidative stress suppresses metastasis of murine melanoma cells, Free Radic. Biol. Med. 129 (2018) 256-267. https://doi.org/10.1016/j.freeradbiomed.2018.07.025.

[30] G.H. Hwang, J.M. Ryu, Y.J. Jeon, et al., The role of thioredoxin reductase and glutathione reductase in plumbagin-induced, reactive oxygen species-mediated apoptosis in cancer cell lines, Eur. J. Pharmacol. 765 (2015) 384-393. https://doi.org/10.1016/j.ejphar.2015.08.058.

[31] G. Asantewaa, I.S. Harris, Glutathione and its precursors in cancer, Curr. Opin. Biotechnol. 68 (2021) 292-299. https://doi.org/10.1016/j.copbio.2021.03.001.

[32] B. Niu, K. Liao, Y. Zhou, et al., Application of glutathione depletion in cancer therapy: enhanced ROS-based therapy, ferroptosis, and chemotherapy, Biomaterials 277 (2021) 121110. https://doi.org/10.1016/j.biomaterials.2021.121110.

[33] S. Hao, B. Liang, Q. Huang, et al., Metabolic networks in ferroptosis, Oncol. Lett. 15 (2018) 5405-5411. https://doi.org/10.3892/ol.2018.8066.

[34] R.M. Pascale, G. Peitta, M.M. Simile, et al., Alterations of methionine metabolism as potential targets for the prevention and therapy of hepatocellular carcinoma, Med. Lith. 55 (2019) 296. https://doi.org/10.3390/medicina55060296.